

Localization effect in single crystal of $RuAs_2$

Zhe-Kai Yi(易哲铠), Qi Liu(刘琪), Shuang-Kui Guang(光双魁), Sheng Xu(徐升), Xiao-Yu Yue(岳小宇), Hui Liang(梁慧), Na Li(李娜), Ying Zhou(周颖), Dan-Dan Wu(吴丹丹), Yan Sun(孙燕), Qiu-Ju Li(李秋菊), Peng Cheng(程鹏), Tian-Long Xia(夏天龙), Xue-Feng Sun(孙学峰), and Yi-Yan Wang(王义炎)

Citation: Chin. Phys. B, 2024, 33 (**4**): 047501. DOI: 10.1088/1674-1056/ad23d9
Journal homepage: http://cpb.iphy.ac.cn; http://iopscience.iop.org/cpb

What follows is a list of articles you may be interested in

Unconventional room-temperature negative magnetoresistance effect in Au/n-Ge:Sb/Au devices

Xiong He(何雄), Fan-Li Yang(杨凡黎), Hao-Yu Niu(牛浩峪), Li-Feng Wang(王立峰), Li-Zhi Yi(易立志),Yun-Li Xu(许云丽), Min Liu(刘敏), Li-Qing Pan(潘礼庆), and Zheng-Cai Xia(夏正才)

Chin. Phys. B, 2024, 33 (**3**): 037504. DOI: 10.1088/1674-1056/ad15f8

Oscillation of Dzyaloshinskii-Moriya interaction driven by weak electric fields

Runze Chen(陈润泽), Anni Cao(曹安妮), Xinran Wang(王馨苒), Yang Liu(柳洋), Hongxin Yang(杨洪新), and Weisheng Zhao(赵巍胜)

Chin. Phys. B, 2024, 33 (**2**): 027501. DOI: 10.1088/1674-1056/ad0f85

Ultrafast antiferromagnet rearrangement in Co/IrMn/CoGd trilayers

Zongxia Guo(郭宗夏), Gregory Malinowski, Pierre Vallobra, Yi Peng(彭懿), Yong Xu(许涌), Stéphane Mangin, Weisheng Zhao(赵巍胜), Michel Hehn, and Boyu Zhang(张博宇)

Chin. Phys. B, 2023, 32 (**8**): 087507. DOI: 10.1088/1674-1056/acda83

Topological magnetotransport and electrical switching of sputtered antiferromagnetic $Ir_{20}Mn_{80}$

Danrong Xiong(熊丹荣), Yuhao Jiang(蒋宇昊), Daoqian Zhu(朱道乾), Ao Du(杜奥), Zongxia Guo(郭宗夏), Shiyang Lu(卢世阳), Chunxu Wang(王春旭), Qingtao Xia(夏清涛), Dapeng Zhu(朱大鹏), and Weisheng Zhao(赵巍胜)

Chin. Phys. B, 2023, 32 (**5**): 057501. DOI: 10.1088/1674-1056/acb9ec

Weak localization in disordered spin-1 chiral fermions

Shaopeng Miao(苗少鹏), Daifeng Tu(涂岱峰), and Jianhui Zhou(周建辉)

Chin. Phys. B, 2023, 32 (**1**): 017502. DOI: 10.1088/1674-1056/ac720b

---

RAPID COMMUNICATION

Localization effect in single crystal of $RuAs_2$

Zhe-Kai Yi(易哲铠)[1], Qi Liu(刘琪)[1], Shuang-Kui Guang(光双魁)[2], Sheng Xu(徐升)[3], Xiao-Yu Yue(岳小宇)[4], Hui Liang(梁慧)[1], Na Li(李娜)[1], Ying Zhou(周颖)[1], Dan-Dan Wu(吴丹丹)[1], Yan Sun(孙燕)[1], Qiu-Ju Li(李秋菊)[5], Peng Cheng(程鹏)[3], Tian-Long Xia(夏天龙)[3,†], Xue-Feng Sun(孙学峰)[1,6,‡], and Yi-Yan Wang(王义炎)[1,§]

[1] *Anhui Key Laboratory of Magnetic Functional Materials and Devices, Institute of Physical Science and Information Technology, Anhui University, Hefei* 230601, *China*

[2] *Department of Physics and Key Laboratory of Strongly-Coupled Quantum Matter Physics (CAS), University of Science and Technology of China, Hefei* 230026, *China*

[3] *Department of Physics and Beijing Key Laboratory of Opto-electronic Functional Materials & Micro-nano Devices, Renmin University of China, Beijing* 100872, *China*

[4] *School of Optical and Electronic Information, Suzhou City University, Suzhou* 215104, *China*

[5] *School of Physics and Optoelectronic Engineering, Anhui University, Hefei* 230601, *China*

[6] *Collaborative Innovation Center of Advanced Microstructures, Nanjing University, Nanjing* 210093, *China*

(Received 6 January 2024; revised manuscript received 19 January 2024; accepted manuscript online 30 January 2024)

We report the magnetotransport and thermal properties of $RuAs_2$ single crystal. $RuAs_2$ exhibits semiconductor behavior and localization effect. The crossover from normal state to diffusive transport in the weak localization (WL) state and then to variable range hopping (VRH) transport in the strong localization state has been observed. The transitions can be reflected in the measurement of resistivity and Seebeck coefficient. Negative magnetoresistance (NMR) emerges with the appearance of localization effect and is gradually suppressed in high magnetic field. The temperature dependent phase coherence length extracted from the fittings of NMR also indicates the transition from WL to VRH. The measurement of Hall effect reveals an anomaly of temperature dependent carrier concentration caused by localization effect. Our findings show that $RuAs_2$ is a suitable platform to study the localized state.

Keywords: weak localization, variable range hopping, $RuAs_2$ single crystal

PACS: 75.47.–m, 72.15.Rn, 71.20.Nr **DOI:** 10.1088/1674-1056/ad23d9

1. Introduction

Localization effect is an important concept in the physics of condensed matter and disordered systems.[1] In the weakly localized region where $kl \gg 1$ (k is the electron wave vector and l is the mean free path), diffusive transport dominates the conductive process. The quantum interference between paths increases the probability of electrons returning to the origin along the closed loop after multiple elastic scattering, that is, enhances the backscattering. The phase shift caused by the magnetic field will suppress the interference and lead to negative magnetoresistance (NMR).[2,3] Weak antilocalization (WAL), an effect opposite to the weak localization (WL), appears as the positive magnetoresistance (MR) with a sharp cusp in low fields.[4,5] WAL is always expected in systems with strong spin–orbit scattering or coupling, in which the strong spin–orbit interaction will lower the probability of backscattering.[6,7] Diffusive transport is absent in the region of strong localization ($kl < 1$). The conductive process is known as variable range hopping (VRH), where the electrons can tunnel between localized states with the assistance of phonons.[2,3]

Transition-metal dipnictides XPn_2 (X = transition metal; Pn = P, As, Sb, Bi) are a large family of materials with rich physical properties. In these materials, $NbAs_2$/$TaAs_2$ are weak topological insulators with extremely large MR, and will evolve into Weyl semimetals under magnetic field.[8–13] WP_2/MoP_2 are type-II Weyl semimetals with extremely high conductivity and MR.[14–17] $FeSb_2$ exhibits colossal Seebeck coefficient and thermoelectric power factor.[18] In addition, superconductivity can be observed in several materials, such as $NbAs_2$ (tip/pressure-induced)[19,20] and $PdBi_2$.[21,22] XPn_2 provides a material platform to explore exotic physical properties.

$RuAs_2$ is a member of transition-metal dipnictide, and its single crystal remains to be synthesized and studied. In this work, we grew the single crystals of $RuAs_2$ and investigated the magnetotransport and thermal properties. The single crystal of $RuAs_2$ is a p-type semiconductor. The localization effect has been found in the samples. With the decrease of temperature, the electron transport can be driven from normal state

†Corresponding author. E-mail: tlxia@ruc.edu.cn
‡Corresponding author. E-mail: xfsun@ahu.edu.cn
§Corresponding author. E-mail: wyy@ahu.edu.cn

© 2024 Chinese Physical Society and IOP Publishing Ltd

to diffusive transport in the WL state, and then to VRH transport in the strong localization state. NMR, as a consequence of WL and VRH, has been clearly observed. The behavior of NMR is consistent with the theoretical prediction. The temperature dependent phase coherence length extracted from the fittings of NMR also indicates the change of conduction mechanism. The Hall resistivity shows the linear behavior of single band. There is an anomaly in the temperature dependent carrier concentration, which is induced by the localization effect. In addition, the specific heat, thermal conductivity and Seebeck coefficient have also been measured. No anomalies were found in the temperature dependent specific heat and thermal conductivity, but the Seebeck coefficient can be influenced by the localized state.

2. Experiment and crystal structure

Single crystals of $RuAs_2$ were grown from tin-fluxes.[23] The starting elements, Ru, As and Sn, were mixed and put into an alumina crucible with a molar ratio of Ru:As:Sn = 1:2:12. The crucible was sealed in a quartz tube and heated to 1150 °C. After that, the quartz tube was cooled to 400 °C at a rate of 3 °C/h, where the Sn flux was removed with a centrifuge. The elemental composition determined by energy dispersive x-ray spectroscopy (EDS, Oxford X-Max 50) was consistent with 1:2 for Ru:As. Powder and single crystal x-ray diffraction (XRD) spectra were measured on a Bruker D8 Advance x-ray diffractometer with Cu K_α radiation. The measurements of magnetotransport properties and specific heat were carried out on a Quantum Design physical property measurement system (QD PPMS-14 T). Thermal conductivity was measured by using a conventional "one heater, two thermometers" technique.[24–28] A RuO_2 chip resistor was used as the heater and attached to the sample by a short gold wire (0.08 mm diameter). The data was measured in a ^{4}He pulse-tube refrigerator and two *in-situ* calibrated Cernox sensors were used as thermometers. The leads for the heater and resistor thermometers on samples were long and thin NbTi superconducting wires (0.01 mm diameter). Seebeck coefficient was measured with a standard one-heater–two-thermometers setup at the same time with the same sample when the thermal conductivity was measured. The 0.025 mm manganin wire was used for all the electrical contacts. Silver epoxy was used to contact the manganin wire and the gold wire. The longitudinal voltage V_{xx} was detected with the nanovoltmeter. Using the x-ray Laue photograph, the sample was cut precisely along the crystallographic axes with typical dimensions of 2.9×0.641×0.152 mm^3, where the longest dimension was along the [110] axis.

$RuAs_2$ crystallizes in space group *Pnnm*. As shown in Figs. 1(a) and 1(b), $RuAs_2$ is composed of twisted $RuAs_6$ octahedrons, which contain two longer and four shorter Ru–As bonds. The grown single crystals are silvery and hard. Figure 1(c) shows the powder XRD pattern of $RuAs_2$ with refinement. The reflections can be well indexed in the space group *Pnnm*. The determined lattice parameters are $a = 5.441$ Å, $b = 6.186$ Å and $c = 2.972$ Å. The weak peaks of tin should come from a small amount of residual flux on the sample surface. The single crystal XRD pattern presented in Fig. 1(d) indicates that the surface of the crystal is (110) plane.

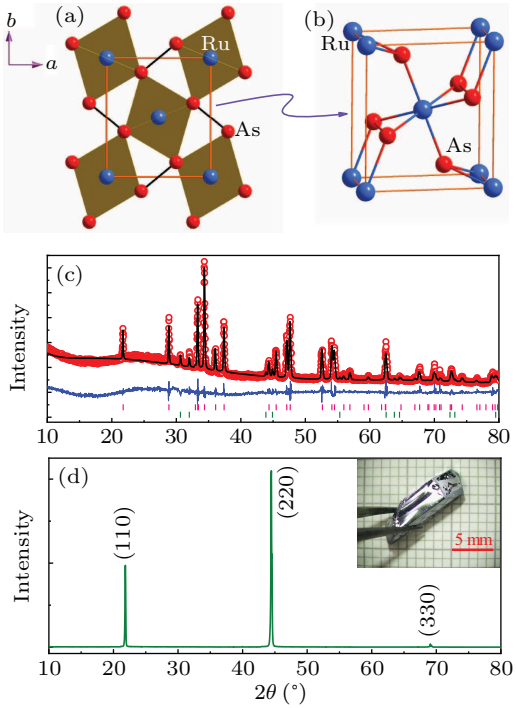


Fig. 1. (a) View of the crystal structure of $RuAs_2$ from *c*-axis direction. (b) Unit cell of the crystal. The blue and red spheres represent Ru and As atoms, respectively. (c) Powder XRD pattern of $RuAs_2$. Black solid line and red circles represent the calculated curve and observed curve, respectively. The difference curve is plotted in the blue line. The vertical pink lines and olive lines denote the positions of Bragg peaks of $RuAs_2$ and Sn, respectively. (d) Single crystal XRD pattern of $RuAs_2$. Inset: a typical image of the grown crystal.

3. Results and discussion

Figure 2(a) plots the temperature dependent resistivity of $RuAs_2$. The resistivity increases with the decrease of temperature, exhibiting a semiconductor behavior. The Arrhenius equation $\rho(T) = \rho_0 \exp(\Delta E/(k_B T))$ (ΔE is the activation energy) is usually used to describe the ρ–T curve of semiconductor. However, as shown in the inset of Fig. 2(a), $\ln\rho$ does not scale linearly with T^{-1} over the entire measured temperature range. Since the Arrhenius equation is not sufficient to describe the behavior of resistivity, the VRH mechanism $\rho(T) = \rho_0 \exp((T_0/T)^{1/(D+1)})$ in D dimensions is employed to understand the conductivity of $RuAs_2$.[29,30] As shown in Fig. 2(b), when the abscissa becomes $T^{-1/4}$, the linear dependence of $\ln\rho$ can be seen clearly. There are two turning points on the curve, indicating the transitions to WL state and VRH state, respectively. The two transition temperatures are 200 K

and 53.4 K. The crossover from WL to VRH can be understood based on the competition between localization length ξ and hopping length $r_{\rm hop}$.[31] Since these two parameters follow $r_{\rm hop}/\xi \approx (T_0/T)^{1/4}$, lowering the temperature makes $r_{\rm hop} \gg \xi$ and drives the system into strong localization.

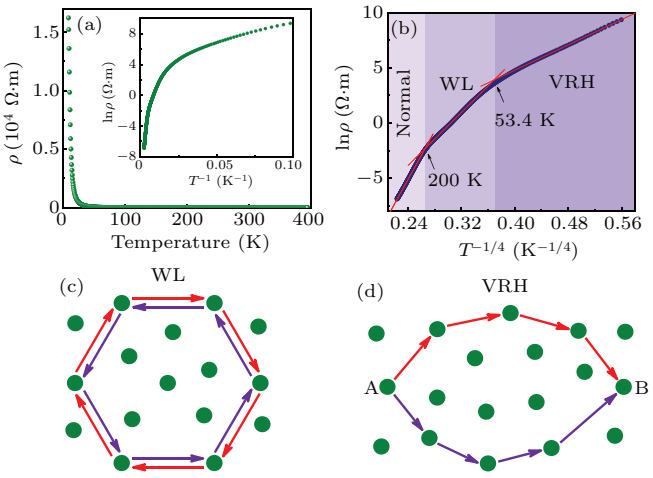


Fig. 2. (a) Temperature dependence of the resistivity of $RuAs_2$ single crystal. Inset: $\ln\rho$ plotted as a function of T^{-1}. (b) $\ln\rho$ plotted as a function of $T^{-1/4}$. (c) and (d) The qualitative pictures of the interference effects in WL model and VRH model, respectively.

Figures 2(c) and 2(d) show the qualitative pictures of WL model and VRH model to describe the physical mechanism and the response on magnetotransport. In the case of WL, the scattered electrons have the probability to return to the origin through a closed path. The probability amplitudes of clockwise path and counterclockwise path will interfere constructively, resulting in the enhancement of backscattering. The application of magnetic field introduces the phase difference between different paths and suppresses the interference, forming the NMR. Unlike the diffusion transport in WL state, carriers in the VRH state can tunnel between localized states, which is a quantum mechanical process. In VRH, the interference occurs between forward paths rather than the paths that circle a loop in WL. This physical mechanism was first proposed by Shklovskii *et al.*, which is called NSS model.[2,32] As shown in Fig. 2(d), the total tunneling amplitude from A to B is the sum of the amplitudes along different paths. Considering a simplified image containing only two paths with amplitudes J_1 and J_2, the conductance in a transverse magnetic field is[33]

$$\sigma_{12}(B) \propto |J_1 + J_2\,\mathrm{e}^{\mathrm{i}\psi}|^2 = J_1^2 + J_2^2 + 2J_1J_2\cos\psi, \qquad (1)$$

where ψ is the phase difference between the two paths caused by magnetic flux. The MR in the VRH region can be positive or negative.[2,33] If all scattering amplitudes are positive ($J_1J_2 > 0$), the interference is constructive and increases the hopping probability from A to B. The suppression of interference by magnetic field will reduce the conductivity, producing a positive MR. If some of the amplitudes are negative ($J_1J_2 < 0$), the interference is destructive, the application of magnetic field will increase the conductivity and produce the NMR.

The transverse MR was measured to confirm the conduction mechanism. As shown in Fig. 3(a), NMR has been observed in the region of localization effect as expected. The NMR emerges at 200 K and becomes more obvious with the decrease of temperature. In a higher magnetic field, the NMR will be suppressed, and the resistivity will increase with increasing the field. The upturn in high field is suggested to be associated with the shrinkage of localized electron wave functions, similar to that observed in other localized systems.[2,31,34]

The magnetoconductivity (MC) $\Delta\sigma = \sigma(B) - \sigma(0)$ due to localization effect can often be satisfactorily described by the Hikami–Larkin–Nagaoka (HLN) equation[35]

$$\Delta\sigma(B) = -\frac{\alpha e^2}{\pi h}\left[\ln\left(\frac{B_\phi}{B}\right) - \psi\left(\frac{1}{2} + \frac{B_\phi}{B}\right)\right], \qquad (2)$$

where $\psi(x)$ is the Digamma function, α is a prefactor, $B_\phi = h/(8e\pi L_\phi^2)$ is the characteristic field, and L_ϕ is the phase coherence length. Figures 3(b) and 3(c) show the low field MC in the WL region and VRH region, both of which can be well fitted by the HLN equation. The phase coherence lengths L_ϕ extracted from the fits are shown in Fig. 3(d). In the region of WL, L_ϕ increases with the decrease of temperature. However, there is a sudden drop below 80 K, indicating the transition from WL to VRH. Overall, the obtained phase coherence lengths of WL and VRH are about in the range of 25–70 nm and 40–50 nm, respectively.

The behavior of MR in VRH can also be qualitatively understood based on the NSS theory.[2] By studying the dependence of localization length ξ on the magnetic field, NSS theory predicts that $\ln[\rho(B)/\rho(0)]$ is proportional to $B^{1/2}$ under moderate field and linearly dependent on B in low field where $r_{\rm hop} \gg \xi$. Figure 3(e) plots $\ln[\rho(B)/\rho(0)]$ as a function of $B^{1/2}$. As indicated by the red solid line, the curve follows $B^{1/2}$ in the moderate field and deviates obviously in low field. The inset of Fig. 3(e) shows the data in low field. The fitting with B^n yields an n of 0.9, indicating that $\ln[\rho(B)/\rho(0)]$ is almost linearly dependent on the field. Thus, the behavior of MR agrees well with the theoretical expectation.

The Hall effect of $RuAs_2$ has also been investigated (Fig. 4). The Hall resistivity is linearly dependent on the magnetic field, showing a single band behavior. The positive slope indicates that $RuAs_2$ is a p-type semiconductor, which is quite different from previous measurement on a polycrystalline pellet.[36] Here, the minimum measurement temperature is 120 K, below which the Hall signal is almost completely suppressed by the transverse MR. A notable feature can be identified from the curves. With the decrease of temperature, the slope increases when $T > 200$ K but decreases when $T < 200$ K. This anomaly corresponds to the emergence of localization effect. Since the Hall coefficient $R_{\rm H} = 1/(en)$,

the anomaly leads to an upturn of carrier concentration below 200 K (Fig. 4(c)). Overall, the carrier concentration is in the order of 10^{16}–10^{19} cm^{-3}. Figure 4(d) shows the carrier mobility calculated by $\mu = 1/(en\rho_{xx}(0\ \mathrm{T}))$. The rapid decrease of mobility at low temperature is mainly related to the large increase of zero-field resistivity.

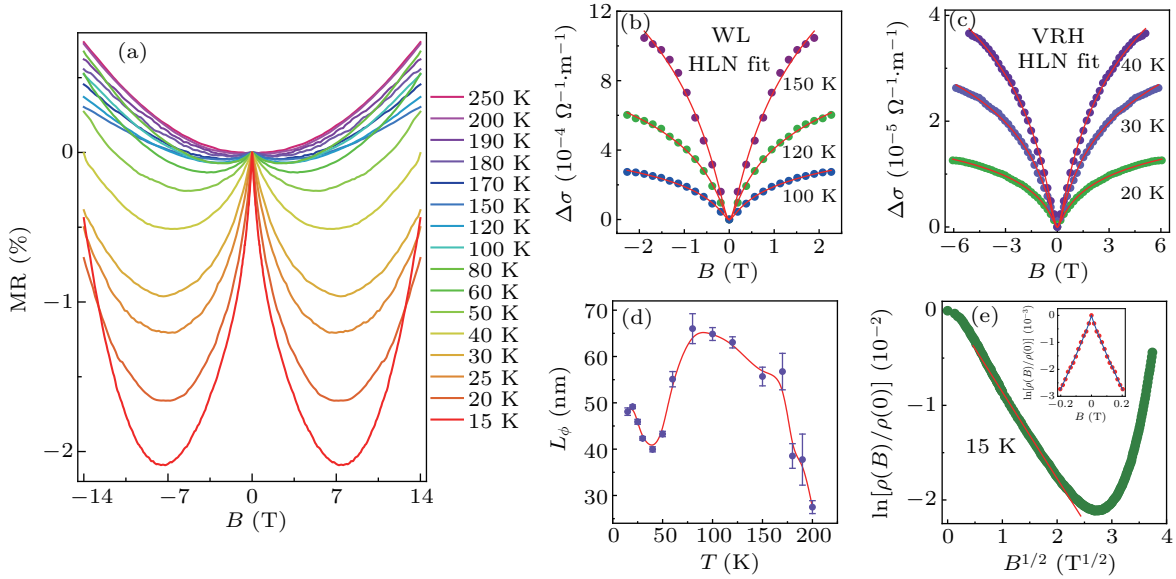


Fig. 3. (a) Magnetic field dependence of the transverse MR at different temperatures. (b) and (c) The HLN fittings of low field MC in WL region and VRH region, respectively. (d) The phase coherence length L_ϕ obtained by fitting. (e) $\ln[\rho(B)/\rho(0)]$ plotted as a function of $B^{1/2}$ at 15 K. Inset: the low field data (points) and the fitting (solid line) with B^n.

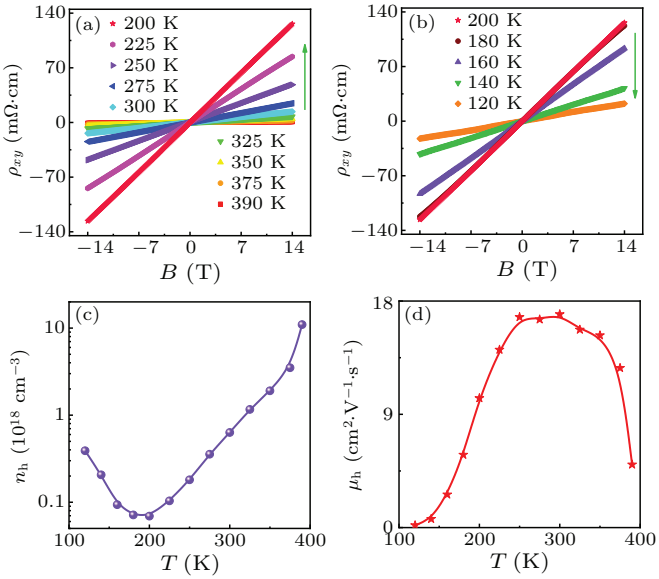


Fig. 4. (a) The field dependent Hall resistivity above 200 K. (b) The field dependent Hall resistivity below 200 K. (c) and (d) The temperature dependent concentration and mobility of hole-type carrier, respectively.

Since the anomaly in Hall effect can also be induced by the structural phase transition,[37,38] the specific heat of $RuAs_2$ was measured to check the possibility of structural phase transition. Figure 5 shows the temperature dependence of specific heat of $RuAs_2$ single crystal. No distinct anomaly is observed around 200 K, excluding the possibility of structural phase transition. The specific heat around room temperature is not very close to the value of Dulong–Petit law, which may be due to the large Debye temperature. The inset plots the C_p/T as a function of T^2 at low temperature, in which the solid line represents the fit with $C_p/T = \gamma + \beta T^2$. The fit yields the values of $\gamma = 0.435$ mJ·mol^{-1}·K^{-2} and $\beta = 0.060$ mJ·mol^{-1}·K^{-4}. The Debye temperature $\Theta_D = 460$ K can be obtained by $\Theta_D = (12\pi^4 NR/(5\beta))^{1/3}$, where R is the gas constant and N is the number of atoms per formula unit.

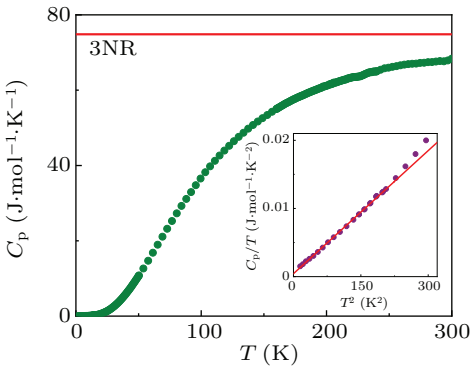


Fig. 5. The temperature dependent specific heat of $RuAs_2$. The solid horizontal line shows the classic value of specific heat at high temperature limit. The inset is the plot of C_p/T vs. T^2, in which the solid line is the linear fit at low temperature.

The thermal conductivity κ and Seebeck coefficient S were measured to find more signals of localized states. As shown in Fig. 6(a), the temperature dependence of κ displays a typical behavior of phonon heat transport with a rather large phonon peak at 33 K and there is no anomaly on the κ–T curve. Figure 6(b) shows the temperature dependence of Seebeck coefficient S. The S decreases with decreasing temperature. After a minimum at 41 K, the S begins to increase sharply. The value of S is up to 3.1 mV/K at 20 K. Although the Seebeck coefficient is large, the figure of merit is small due to the large resistivity and thermal conductivity. It

is worth noting that there is a broad kink on the curve. Figure 6(c) presents the plot of dS/dT against temperature to understand the kink. The two peaks indicate two slope transition points on the S–T curve. Interestingly, the two slope transitions occur around 53 K and 200 K, which is consistent with the transitions observed in resistivity (Fig. 2(b)). Obviously, the slope transitions on the S–T curve reveal the influence of WL and VRH on Seebeck coefficient. In addition, the Seebeck coefficient has a sign change in the range of 34–63 K (see the inset in Fig. 6(b)). Similar behavior can also be found in $Fe_{1+x}Te_{1-y}Se_y$[39] and $FeGe_2$.[40] In general, the Seebeck coefficient can be described by the Mott formula[39,41]

$$S = \frac{\pi^2 k_B^2 T}{3e}\left[\frac{\mathrm{d}\ln\sigma(E)}{\mathrm{d}E}\right] \approx \frac{\pi^2 k_B^2 T}{3e}\left(\frac{N}{n} + \frac{1}{\tau}\frac{\mathrm{d}\tau}{\mathrm{d}E}\right), \quad (3)$$

where σ, k_B, N, n and τ are the conductivity, Boltzmann constant, density of states, carrier concentration and scattering time, respectively. Usually, S has the same sign as the carrier due to the dominance of the first term in Eq. (3). The sign change of S indicates the change of carrier type. However, if the scattering mechanism changes suddenly, the second term in Eq. (3) may have a great influence on S. The second term is negative ($\tau \propto E^{-\alpha}$, $\alpha > 0$), and S has the possibility of changing the sign.[39] Since the Hall effect is absent in this temperature region, the origin of the sign change of S remains to be clarified.

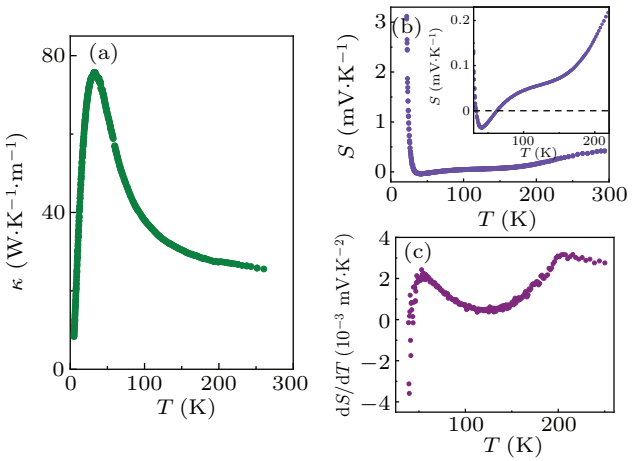


Fig. 6. (a) and (b) The temperature dependent thermal conductivity and Seebeck coefficient, respectively. The inset of (b) shows the enlarged part of 30–220 K. (c) dS/dT plotted as a function of temperature.

4. Summary

In summary, single crystals of $RuAs_2$ are grown and the magnetotransport and thermal properties have been studied. The resistivity shows a semiconductor behavior. The analysis of resistivity reveals the crossover from normal state to weak localized state and then to strong localized state. The signal of transition can also be found in the measurement of Seebeck coefficient. In the region of localization effect, NMR can be observed and well understood based on WL model and VRH model. The phase coherence lengths have been extracted from the fits of NMR. In addition, an anomaly caused by the localization effect appears in the temperature dependent carrier concentration.

Acknowledgements

Project supported by the National Key Research and Development Program of China (Grant Nos. 2023YFA1406500 and 2019YFA0308602), the National Natural Science Foundation of China (Grant Nos. 12104011, 12274388, 12074425, 52102333, 12104010, 12204004, and 11874422), and the Natural Science Foundation of Anhui Province (Grant Nos. 2108085QA22 and 2108085MA16).

References

[1] Abrahams E 2010 *50 years of Anderson Localization* (Singapore: World Scientific)
[2] Ioffe L and Spivak B 2013 *J. Exp. Theor. Phys.* **117** 551
[3] Zhang L, King I, Nasyedkin K, Chen P, Skinner B, Lunt R R and Pollanen J 2021 *ACS Appl. Electron. Mater.* **3** 2948
[4] Huang X, Zhao L, Long Y, Wang P, Chen D, Yang Z, Liang H, Xue M, Weng H, Fang Z, Dai X and Chen G 2015 *Phys. Rev. X* **5** 031023
[5] Lang M, He L, Kou X, Upadhyaya P, Fan Y, Chu H, Jiang Y, Bardarson J H, Jiang W, Choi E S, *et al.* 2013 *Nano Lett.* **13** 48
[6] Lu H Z and Shen S Q 2011 *Phys. Rev. B* **84** 125138
[7] Lu H Z, Shi J and Shen S Q 2011 *Phys. Rev. Lett.* **107** 076801
[8] Wang Y Y, Yu Q H, Guo P J, Liu K and Xia T L 2016 *Phys. Rev. B* **94** 041103(R)
[9] Wu D, Liao J, Yi W, Wang X, Li P, Weng H, Shi Y, Li Y, Luo J, Dai X, *et al.* 2016 *Appl. Phys. Lett.* **108** 042105
[10] Yuan Z, Lu H, Liu Y, Wang J and Jia S 2016 *Phys. Rev. B* **93** 184405
[11] Shen B, Deng X, Kotliar G and Ni N 2016 *Phys. Rev. B* **93** 195119
[12] Luo Y, McDonald R, Rosa P, Scott B, Wakeham N, Ghimire N, Bauer E, Thompson J and Ronning F 2016 *Sci. Rep.* **6** 27294
[13] Gresch D, Wu Q, Winkler G W and Soluyanov A A 2017 *New J. Phys.* **19** 035001
[14] Kumar N, Sun Y, Xu N, Manna K, Yao M, Süss V, Leermakers I, Young O, Förster T, Schmidt M, *et al.* 2017 *Nat. Commun.* **8** 1642
[15] Razzoli E, Zwartsenberg B, Michiardi M, Boschini F, Day R P, Elfimov I S, Denlinger J D, Süss V, Felser C and Damascelli A 2018 *Phys. Rev. B* **97** 201103(R)
[16] Wang A, Graf D, Liu Y, Du Q, Zheng J, Lei H and Petrovic C 2017 *Phys. Rev. B* **96** 121107(R)
[17] Lv Y Y, Li X, Zhang J, Pang B, Chen S S, Cao L, Zhang B B, Lin D, Chen Y B, Yao S H, Zhou J, Zhang S T, Lu M H, Tian M and Chen Y F 2018 *Phys. Rev. B* **97** 245151
[18] Bentien A, Johnsen S, Madsen G, Iversen B and Steglich F 2007 *Europhys. Lett.* **80** 17008
[19] Zhang M D, Hou X Y, Wang Q, Wang Y Y, Zhao L X, Wang Z, Gu Y D, Zhang F, Xia T L, Ren Z A, Chen G F, Hao N and Shan L 2020 *Phys. Rev. B* **102** 085139
[20] Li Y, An C, Hua C, Chen X, Zhou Y, Zhou Y, Zhang R, Park C, Wang Z, Lu Y, *et al.* 2018 *npj Quantum Mater.* **3** 1
[21] Chen J, Wang A, Pang G, Su H, Chen Y and Yuan H 2020 *Phys. Rev. B* **101** 054514
[22] Dimitri K, Hosen M M, Dhakal G, Choi H, Kabir F, Sims C, Kaczorowski D, Durakiewicz T, Zhu J X and Neupane M 2018 *Phys. Rev. B* **97** 144514
[23] Bugaris D E, Malliakas C D, Shoemaker D P, Do D T, Chung D Y, Mahanti S D and Kanatzidis M G 2014 *Inorg. Chem.* **53** 9959
[24] Sun X F, Tao W, Wang X M and Fan C 2009 *Phys. Rev. Lett.* **102** 167202
[25] Zhou H D, Zhao Z Y, Sun X F, Nieto Suarez M, Rivas-Murias B, Tsurkan V, Deisenhofer J, Zapf V S and Rivadulla F 2013 *Phys. Rev. B* **87** 174436

[26] Zhao Z Y, Tong B, Zhao X, Chen L M, Shi J, Zhang F B, Song J D, Li S J, Wu J C, Xu H S, Liu X G and Sun X F 2015 *Phys. Rev. B* **91** 134420

[27] Shen S P, Wu J C, Song J D, Sun X F, Yang Y F, Chai Y S, Shang D S, Wang S G, Scott J F and Sun Y 2016 *Nat. Commun.* **7** 10569

[28] Gu C C, Zhao Z Y, Chen X L, Lee M, Choi E S, Han Y Y, Ling L S, Pi L, Zhang Y H, Chen G, Yang Z R, Zhou H D and Sun X F 2018 *Phys. Rev. Lett.* **120** 147204

[29] Abramchuk M, Ozsoy-Keskinbora C, Krizan J W, Metz K R, Bell D C and Tafti F 2017 *J. Am. Chem. Soc.* **139** 15371

[30] Medina E, Kardar M and Rangel R 1996 *Phys. Rev. B* **53** 7663

[31] Liao J, Ou Y, Feng X, Yang S, Lin C, Yang W, Wu K, He K, Ma X, Xue Q K and Li Y 2015 *Phys. Rev. Lett.* **114** 216601

[32] Nguyen V, Spivak B and Shklovskii B 1985 *Sov. Phys. JETP* **62** 1021

[33] Shklovskii B and Spivak B 1991 *Scattering and Interference Effects in Variable Range Hopping* (Amsterdam: Elsevier Science Publishers)

[34] Jiang H W, Johnson C E and Wang K L 1992 *Phys. Rev. B* **46** 12830

[35] Hikami S, Larkin A I and Nagaoka Y 1980 *Prog. Theor. Phys.* **63** 707

[36] Fischer K F, Jørgensen L R, Reardon H, Zhang J and Iversen B B 2018 *Phys. Chem. Chem. Phys.* **20** 9930

[37] Wang Y Y, Zhong C, Li M, Zhu W L, Hou W J, Song W H, Dong Q X, Huang Y F, Zhang S, Ren Z A, Wang S and Chen G F 2020 *Phys. Rev. B* **102** 115122

[38] Yan J Q, Kreyssig A, Nandi S, Ni N, Bud'ko S L, Kracher A, McQueeney R J, McCallum R W, Lograsso T A, Goldman A I and Canfield P C 2008 *Phys. Rev. B* **78** 024516

[39] Pallecchi I, Lamura G, Tropeano M, Putti M, Viennois R, Giannini E and Van der Marel D 2009 *Phys. Rev. B* **80** 214511

[40] Hashizume M, Yokouchi T, Nakagawa K and Shiomi Y 2021 *Phys. Rev. B* **104** 115109

[41] Mott N F 1987 *Conduction in Non-Crystalline Materials* (Oxford: Clarendon)